Acta Materialia 266 (2024) 119653

Contents lists available at ScienceDirect

Acta Materialia

journal homepage: www.elsevier.com/locate/actamat

Full length article

Vacancy diffusion barrier spectrum and diffusion correlation in multicomponent alloys

Bin Xing [a], Wanjuan Zou [b], Timothy J. Rupert [a,b], Penghui Cao [b,a,*]

[a] Department of Material Science and Engineering, University of California, Irvine, CA 92697, United States
[b] Department of Mechanical and Aerospace Engineering, University of California, Irvine, CA 92697, United States

ARTICLE INFO

Keywords:
Defects
Diffusion
Diffusion correlation
High-entropy alloys
Neural network

ABSTRACT

Vacancy diffusion serves a crucial role in many important kinetic behaviors and properties of multicomponent alloys. Essential questions, however, persist regarding how chemical complexity affects diffusion and what unique characteristics, if any, set these alloys apart from traditional metals. Using neural network kinetics model, we study vacancy diffusion in NbMoTa alloy across a broad temperature range (2600 to 800 K). Unlike pure metals, the two key diffusion parameters—diffusion correlation factor f and activation energy ΔG_m—are not constant in alloys, but instead substantially decrease with decreasing temperature. This temperature dependence arises from a reduced number of active vacancy jump pathways at lower temperatures, leading to more correlated diffusion. Upon examining vacancy diffusion throughout the entire compositional space of the Nb-Mo-Ta system, we discover that the slowest vacancy diffusion surprisingly occurs in the non-equimolar region, rather than the equimolar concentration where the configurational entropy is highest. The diffusion barrier spectrum, characterizing the diffusion energy landscape, is an intrinsic material characteristic, which controls both f and ΔG_m and, thereby, the diffusivity. Finally, we find that the vacancy diffusion rate drops noticeably in the presence of local chemical order in the NbMoTa system, particularly for MoTa alloys with long-range B2 order.

1. Introduction

Diffusion transporting atoms from one point to another controls a variety of kinetic processes or behaviors, such as precipitation [1], phase nucleation [2], and radiation-induced void formation [3]. From a microscopic perspective, diffusion in crystalline solids stems from thermally-activated atomic jumps between nearest neighboring sites that are mediated by lattice defects such as vacancies (vacancy mechanism) [4]. This enables a description of the vacancy diffusivity, or diffusion rate, through physical quantities pertaining to the inherent material properties, defined as $D = f\lambda^2 Z\nu_0 \exp(-\Delta E_m/k_B T)/6$, where λ, Z, ν_0, k_B, and T denote the jump distance, coordination number, attempt frequency, Boltzmann constant, and temperature, respectively [4]. In this equation, f and ΔE_m, representing diffusion correlation factor and vacancy migration energy barrier, are the two decisive parameters determining vacancy diffusivity at a given temperature. In pure metals, there is a unique migration barrier associated with each jump pathway on a smooth diffusion energy landscape [5,6]. Vacancy jumps towards each nearest neighboring site occur at the same rate, giving rise to the uncorrelated lattice jump (random walk) characterized by a constant correlation factor, f. In contrast, local chemical fluctuations, particularly in multicomponent alloys, alter the energy barriers along different pathways. This results in a broad distribution of migration barriers (spectrum) and a rugged energy landscape [7–9]. Given the vast compositional scope of a multicomponent alloy [10,11], it remains unclear how the chemical complexity and chemical ordering influence f and ΔE_m that have such a pivotal role in vacancy diffusivity.

The emergence of multi-principal element alloys (MPEAs), commonly known as high entropy alloys (HEAs) [12,13], has attracted increasing attention due to some of the extraordinary properties, including high-temperature strength [14,15], high corrosion resistance [16], and enhanced radiation tolerance [17]. These properties are closely related to, if not fully determined by, diffusion. Mainly motivated by the high entropy concept and consciously circumventing the challenges posed by the vast compositional space, research has been concentrated on the equimolar concentration of HEAs [10,18]. The concept of "sluggish diffusion" [19], suggesting slower diffusion kinetics in HEAs compared to their constituent components, has sparked a decade-long discussion about the role of configurational entropy [19–30]. The original hypothesis behind this concept is that the

* Corresponding author.
E-mail address: caoph@uci.edu (P. Cao).

https://doi.org/10.1016/j.actamat.2024.119653
Received 7 August 2023; Received in revised form 26 December 2023; Accepted 4 January 2024
Available online 5 January 2024

diffusion activation energy is positively related to the number of composing elements in the alloy that accounts for the sluggish diffusion [19]. The high-dimensional compositional space that an MPEA holds and the local chemical complexity pose a grand challenge to our fundamental understanding of vacancy diffusion in these materials.

In this study, we aim to elucidate the interplay between vacancy diffusion and chemical complexity in multicomponent alloys. By employing a recently formulated vacancy jump-resolved neural network kinetics model [31] and a ternary Nb-Mo-Ta system, we find that diffusion correlation factor, f, and activation energy, ΔG_{m}, significantly decrease with a reduction in temperature from 2600 to 800 K. By exploring vacancy diffusivity across the entire ternary compositional space, we determine that the composition with the lowest diffusivity is not equimolar. Furthermore, we demonstrate that the inherent diffusion barrier spectrum, a material constant that depicts the underlying diffusion energy landscape, regulates diffusivity by governing both f and ΔG_{m}. Lastly, we reveal that the presence of chemical short-range order in Nb-Mo-Ta alloy reduces vacancy diffusivity. This decrease becomes even more pronounced in Mo-Ta alloys that exhibit long-range B2 order.

2. Methods

2.1. Material model and diffusion barrier calculation

We study the refractory Nb-Mo-Ta as the model system to demonstrate vacancy diffusion behaviors in multicomponent alloys. To create vacancy barrier datasets for training neural networks, we use atomic models that have a size of 10 × 10 × 10 unit cells, containing 2000 atoms. The climbing image nudged elastic band (CI-NEB) [32] method is adopted to compute the saddle point and vacancy migration barrier in the Nb-Mo-Ta alloys using a machine learning potential [33]. For a configuration of a vacancy, eight final configurations are prepared by swapping the vacancy with its first nearest neighboring atoms. This allows us to label and prepare each diffusion path, creating path-dependent diffusion energy barriers. Prior to the CI-NEB calculation, both the initial and final configurations are optimized to reach their respective local energy minimum states. The CI-NEB inter-replica spring constant is set to be 5 eV/Å^2, and the energy tolerance and force tolerance are 0 eV and 0.01 eV/Å, respectively. The choice of parameters that optimize convergence of the calculations results in essentially the same energy barrier using smaller tolerance and large spring constant. When modeling vacancy diffusions, we use relatively large atomic models of 40 × 40 × 40 unit cells (containing 128,000 atoms). In Sections 3–5, the models for the alloys are prepared as random solid solutions. In Section 6, we use the equimolar NbMoTa model with short-range order, generated from neural network kinetic Monte Carlo with 10 million vacancy jumps.

2.2. Vacancy migration barrier prediction

We construct a neural network to predict vacancy barriers in atomic configurations and alloy compositions. The network consists of 4 hidden layers, with 128 neurons in each layer. To train this model, we created datasets from forty-six distinct compositions, uniformly distributed within the ternary Nb-Mo-Ta space [31]. This sampling strategy is designed to provide the neural network with a broad spectrum of composition concentrations, enhancing its ability to generalize and perform effectively on previously unseen compositions. For each composition, we compute 16,000 barrier data points. Fig. 1a compares the predicted migration barriers with the calculated values from CI-NEB on the equimolar NbMoTa, $Nb_{20}Mo_{60}Ta_{20}$, and $Nb_{10}Mo_{10}Ta_{80}$, respectively. The test results on the new compositions and configurations show a notable prediction performance of the neural network model. We train a series of neural networks with varying number of layers and number of neurons in each layer, to understand the influence of network architecture on prediction performance. Further details on this aspect are elaborated on here [31]. Fig. 2a-b presents the predicted diffusion barrier diagram for Nb-Mo-Ta, using color coding to indicate the mean barrier and standard deviation, respectively. Given the high efficiency and accuracy of the model in predicting migration barriers, we can effectively calculate the vacancy diffusivities throughout the entire ternary space.

2.3. Neural network kinetic Monte Carlo

Vacancy diffusion is performed using the kinetic Monte Carlo algorithm with the vacancy barriers predicted from the neural network [31]. Diffusion occurs through a vacancy jumping to its nearest neighbor sites, each of which with a rate defined as $k_i = k_0 exp(-\Delta E_{\mathrm{m},i}/k_{\mathrm{B}}T)$, where k_0, k_{B}, T denotes the attempt frequency, Boltzmann constant, and temperature, respectively. In this equation, the $\Delta E_{\mathrm{m},i}$ represents the vacancy migration barrier along the jump path i. The accurate migration barriers associated with the eight jump paths in Nb-Mo-Ta alloys are effectively obtained from neural network. The total jump rate R is the sum of all individual elementary rate, $R = \sum_{i=1}^{8} k_i$. To simulate the vacancy jump, we first draw a uniform random number $u \in (0, 1]$ and select a migration path p, which satisfies the condition [34], $\sum_{i=1}^{p-1} k_i/R \le u \le \sum_{i=1}^{p} k_i/R$. The vacancy jump along path p is executed through the exchange between the vacancy and the selected neighboring atom.

3. Vacancy diffusion correlation and the correlation factor

Vacancy diffusion in crystalline solids occurs through a sequence of jumps from one lattice site to its neighboring sites. The net displacement, $\boldsymbol{R}$, of a vacancy after n jumps is defined as, $\boldsymbol{R} = \sum_{i=1}^{n} \boldsymbol{r}_i$, where $\boldsymbol{r}_i$ denotes the displacement vector of ith jump. The square magnitude of

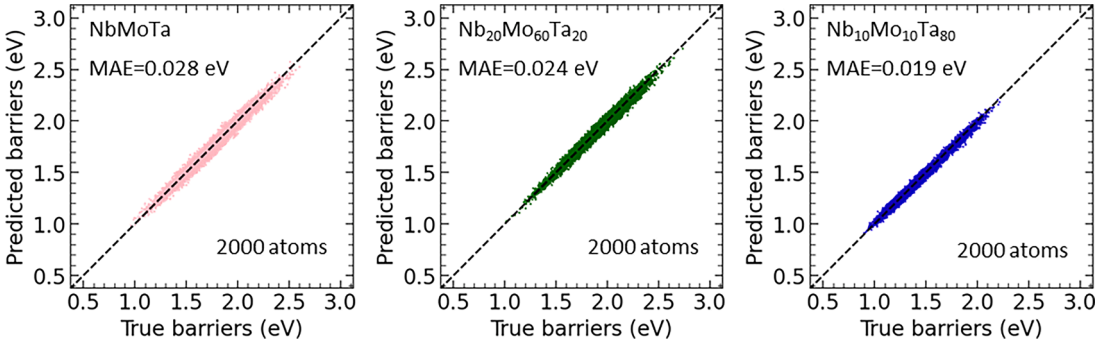

Fig. 1. Testing of the neural network in predicting vacancy migration energy barriers in three compositions, including the equimolar NbMoTa, $Nb_{20}Mo_{60}Ta_{20}$ and $Nb_{10}Mo_{10}Ta_{80}$. The prediction error is measured by the mean absolute error.

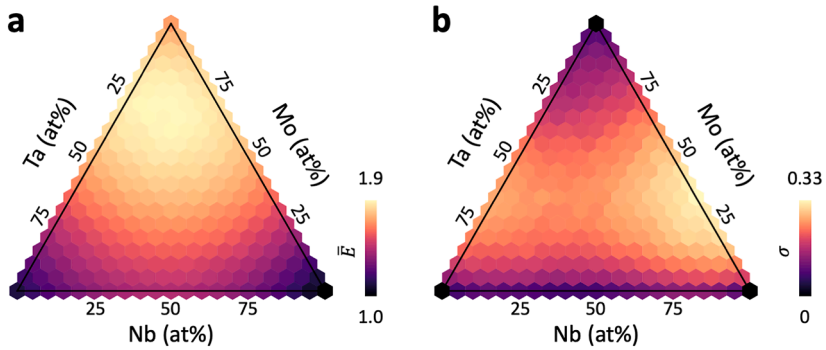

Fig. 2. (a-b) demonstrate the predicted mean and standard deviation of the vacancy migration barrier spectra across the ternary space.

the net displacement, $\boldsymbol{R}^2$, can be formulated as $\boldsymbol{R}^2 = (\sum_{i=1}^{n} \boldsymbol{r}_i)^2 = \sum_{i=1}^{n} \boldsymbol{r}_i^2 + 2\sum_{i=1}^{n-1}\sum_{j=i+1}^{n} \boldsymbol{r}_i \boldsymbol{r}_j$. When considering jumps to the first nearest neighbor site at a constant distance, the squared displacement $\boldsymbol{R}^2$ can be written as $\boldsymbol{R}^2 = n\lambda^2 + 2\lambda^2 \sum_{i=1}^{n-1}\sum_{j=i+1}^{n} \cos\theta_{ij}$, where λ represents the jump distance or first nearest neighbor distance, and θ_{ij} denotes the angle between ith and jth jumps. By averaging $\boldsymbol{R}^2$ over the ensemble, we obtain the mean square displacement (MSD), $\langle \boldsymbol{R}^2 \rangle = \langle n \rangle \lambda^2 + 2\lambda^2 \sum_{i=1}^{n-1}\sum_{j=i+1}^{n} \langle \cos\theta_{ij} \rangle$. In the equation, the first term $\langle n \rangle \lambda^2$, named as accumulative mean square displacement (aMSD) $\langle \boldsymbol{R}_a^2 \rangle$, represents the mean square of all individual jump displacements [7]. The second term $2\lambda^2 \sum_{i=1}^{n-1}\sum_{j=i+1}^{n} \langle \cos\theta_{ij} \rangle$ takes into account the influence of the angle between each pair of jumps, reflecting jump correlation. For random or uncorrelated diffusion, such as diffusion in a pure metal, each jump is independent of all historical jumps and the double sum term reduces to zero because on average $\cos\theta_{ij}$ can have an equal chance of being negative and positive, making both MSD and aMSD equivalent and equal to $\langle n \rangle \lambda^2$. In the case of non-random diffusion where correlation between jumps exists due to positional memory effect [4], the double sum term becomes negative, leading to the decrease in $\langle \boldsymbol{R}^2 \rangle$ (i.e., the net diffusion distance). The diffusion correlation factor, defined as the ratio between $\langle \boldsymbol{R}^2 \rangle$ and $\langle \boldsymbol{R}_a^2 \rangle$ as, $f = 1 + 2\sum_{i=1}^{n-1}\sum_{j=i+1}^{n} \langle \cos\theta_{ij} \rangle / n = \langle \boldsymbol{R}^2 \rangle / \langle \boldsymbol{R}_a^2 \rangle$, is to quantify the degree of diffusion correlation. Having access to both $\langle \boldsymbol{R}^2 \rangle$ and $\langle \boldsymbol{R}_a^2 \rangle$ in the neural network kinetics method, we can compute f accurately and evaluate the role of chemical complexity in diffusion correlation .

Fig. 3a presents the vacancy diffusion trajectories in pure Nb after performing 400 jumps at a wide range of temperatures, for 2600, 800, and 400 K, from kinetic Monte Carlo based on our neural network kinetics model. We conduct five independent simulations at each temperature, resulting in five trajectories, denoted by various colors in the figure. Notably, the vacancies have effectively migrated across a large

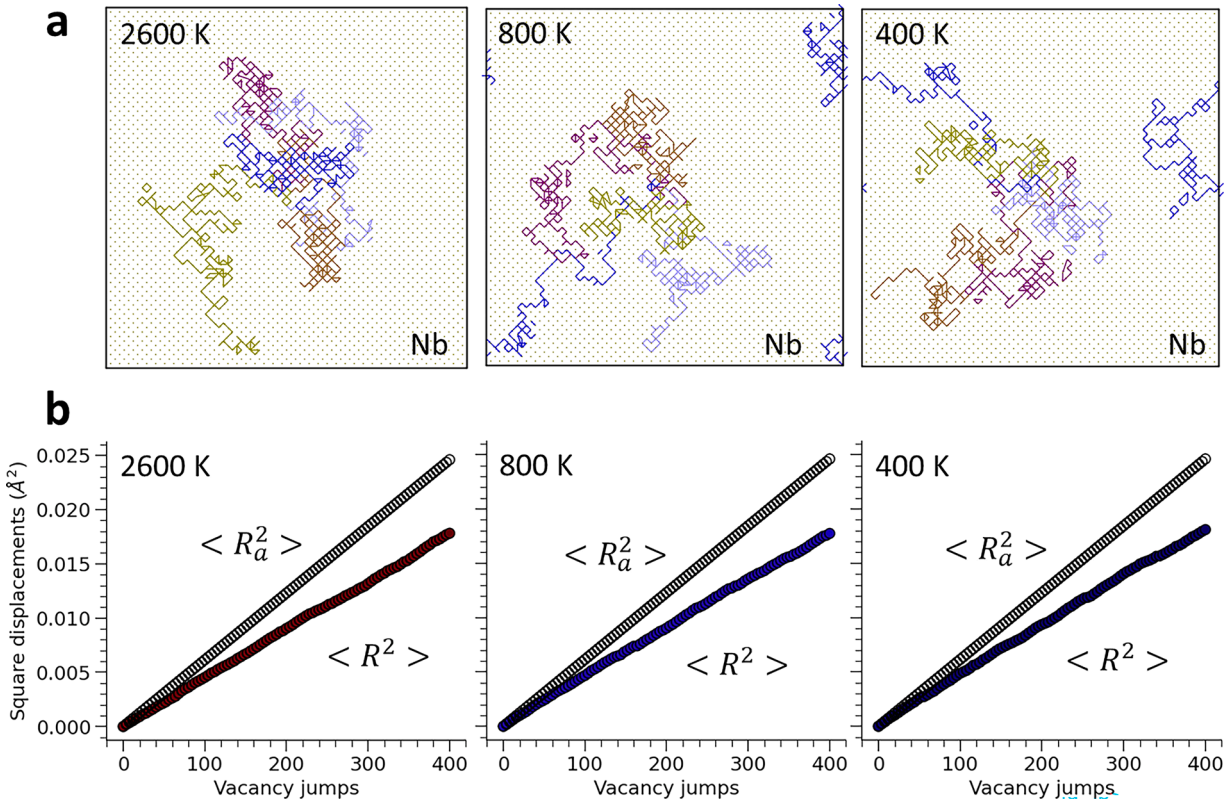

Fig. 3. Vacancy diffusion behavior in pure Nb. (a) The recorded diffusion trajectories of five individual vacancies at 2600, 800, and 400 K after 400 atom jumps. Different colors correspond to different vacancies. (b) The corresponding mean square displacement $\langle \boldsymbol{R}^2 \rangle$ and accumulative mean square displacement $\langle \boldsymbol{R}_a^2 \rangle$ as a function of vacancy jumps.

region after 400 jumps especially at high temperatures. Fig. 3b illustrates the two square displacements, $\langle \boldsymbol{R}^2 \rangle$ and $\langle \boldsymbol{R}_a^2 \rangle$, as a function of vacancy jumps. The value of $\langle \boldsymbol{R}^2 \rangle$ is slightly smaller than $\langle \boldsymbol{R}_a^2 \rangle$, suggesting a high degree of diffusion uncorrelation (i.e., a larger diffusion correlation factor). The range of $\langle \boldsymbol{R}^2 \rangle$ remains relatively constant across different temperatures (Fig. 3b), implying a temperature-independent diffusion correlation. For comparison, we perform the same vacancy diffusion simulations in the equimolar NbMoTa. Fig. 4a illustrates the vacancy trajectories after the same number of 400 jumps at 2600, 800 and 400 K. In contrast to pure Nb, the trajectories exhibit a very noticeable decrease in migration distance as the temperature is lowered. At 400 K, the trajectories are substantially shortened, indicating vacancies have only traveled a short distance after 400 jumps. In Fig. 4b, we highlight the $\langle \boldsymbol{R}^2 \rangle$ values at the three corresponding temperatures. It's evident that the $\langle \boldsymbol{R}^2 \rangle$ values decrease at lower temperatures, suggesting a temperature-dependent diffusion correlation.

Fig. 5 presents the diffusion results over a temperature range from 2600 to 800 K, to investigate the temperature dependence of the correlation factor. Fig. 5a illustrates the variation of $\langle \boldsymbol{R}^2 \rangle$ and $\langle \boldsymbol{R}_a^2 \rangle$ as a function of diffusion jumps for Nb, with the $\langle \boldsymbol{R}^2 \rangle$ curves color-encoded by their corresponding temperatures. The overlapping of $\langle \boldsymbol{R}^2 \rangle$ signifies that the diffused square displacement of vacancy is essentially constant in Nb as temperature varies. In NbMoTa, however, the $\langle \boldsymbol{R}^2 \rangle$ exhibits a clear decrease with decreasing temperature, as depicted in Fig. 5b. To compute the diffusion correlation factor f in NbMoTa alloy, we performed a much longer simulation, accessing 1 million jumps, to ensure that vacancies diffused over a large distance to sample different chemical environments. The resulting correlation factors, $f = \langle \boldsymbol{R}^2 \rangle / \langle \boldsymbol{R}_a^2 \rangle$, are shown in Fig. 5c, for both Nb and NbMoTa. For Nb, the value of f remains a constant of 0.73, which is consistent with the theoretical value for vacancy diffusion in body-centered cubic (bcc) lattice [35,36], verifying our model and the random-walk nature of lattice diffusion in this pure metal. Intriguingly, the correlation factor in NbMoTa varies extensively with temperature, from 0.50 at 2600 K to 0.03 at 800 K (decreasing by more than one order of magnitude). This strong temperature dependence indicates an intensified diffusion correlation at lower temperatures for the MPEA.

From a microscopic perspective, the diffusion correlation stems from the relationship between the current jump and previous jumps. For random-walk lattice diffusion, the vacancy jump along each direction has the same rate, which is independent of the previous jumps (i.e., there is no memory effect). Therefore, all directions have the equivalent jump probability, $1/Z$, where Z denotes the coordination number (where $Z = 8$ for bcc). The chance for a vacancy to return to its previous site (backward jump probability) also equals $1/Z$. Noted that a backward jump will cancel the previous jump and decreases the effectiveness of jumps and the value of $\langle \boldsymbol{R}^2 \rangle$). In alloys, however, the backward jump probability depends on the local chemical environment and system temperature, which exhibits a distribution. Fig. 5d denotes this distribution of backward jump probability, collected from 50,000 diffusion jumps at 800, 1400, and 2600 K. At the high temperature of 2600 K, the backward probability shows a peak value around 1/8, indicating a random-walk like nature. With decreasing temperature from 1400 to 800 K, we can see that the backward jump probability increases and approaches a value of 0.95 at 800 K. This means at low temperatures the vacancy has an increased chance to diffuse back, which reflects the predominated role of low barrier diffusion paths. The enhanced occurrence of back and forth jump lowers the jump effectiveness and reduce the mean squared displacement, $\langle \boldsymbol{R}^2 \rangle$, which is the mechanistic origin of improved diffusion correlation at lower temperatures (i.e., a smaller value of f).

4. Diffusivity and effective diffusion barrier

The temperature-dependent diffusivity of traditional metals is frequently described by an Arrhenius equation associated with thermal-

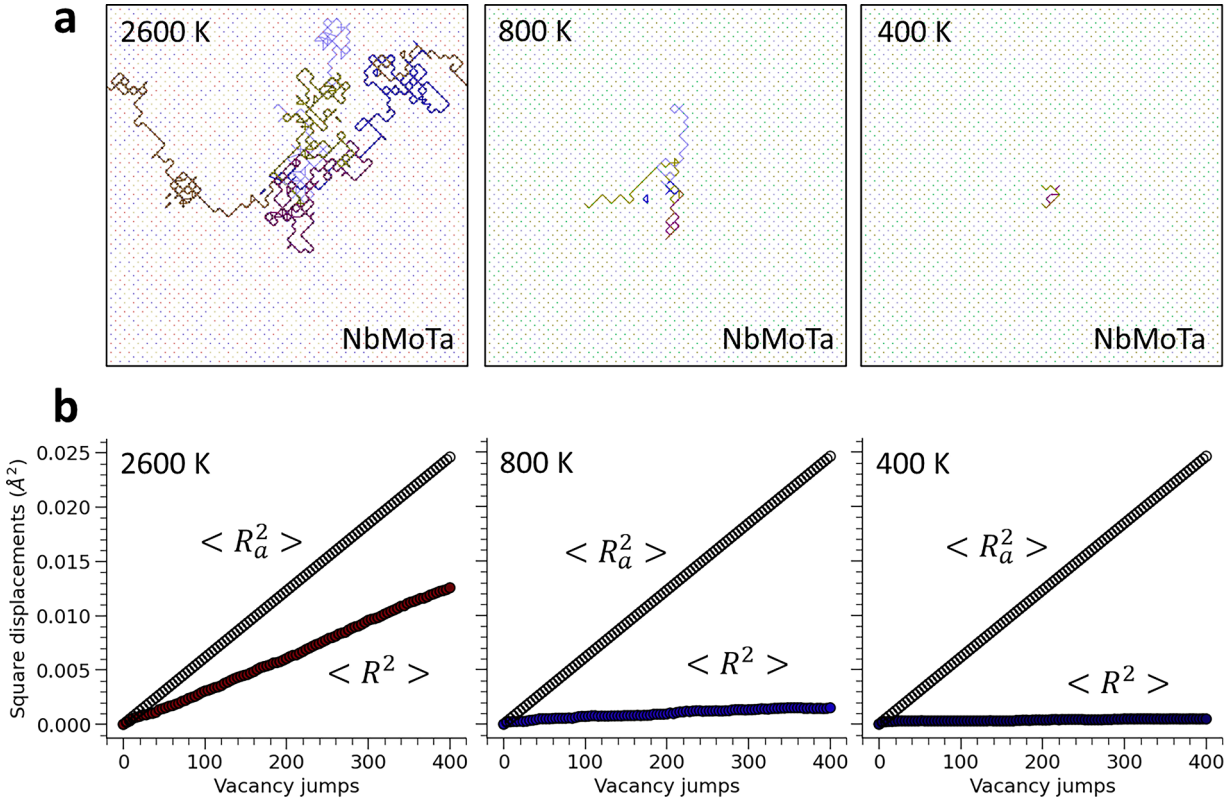

Fig. 4. Vacancy diffusion behavior in equimolar NbMoTa alloy. (a) The recorded diffusion trajectories of five individual vacancies at 2600, 800, and 400 K after 400 atom jumps. (b) The corresponding mean square displacement $\langle \boldsymbol{R}^2 \rangle$ and accumulative mean square displacement $\langle \boldsymbol{R}_a^2 \rangle$as a function of vacancy jumps.

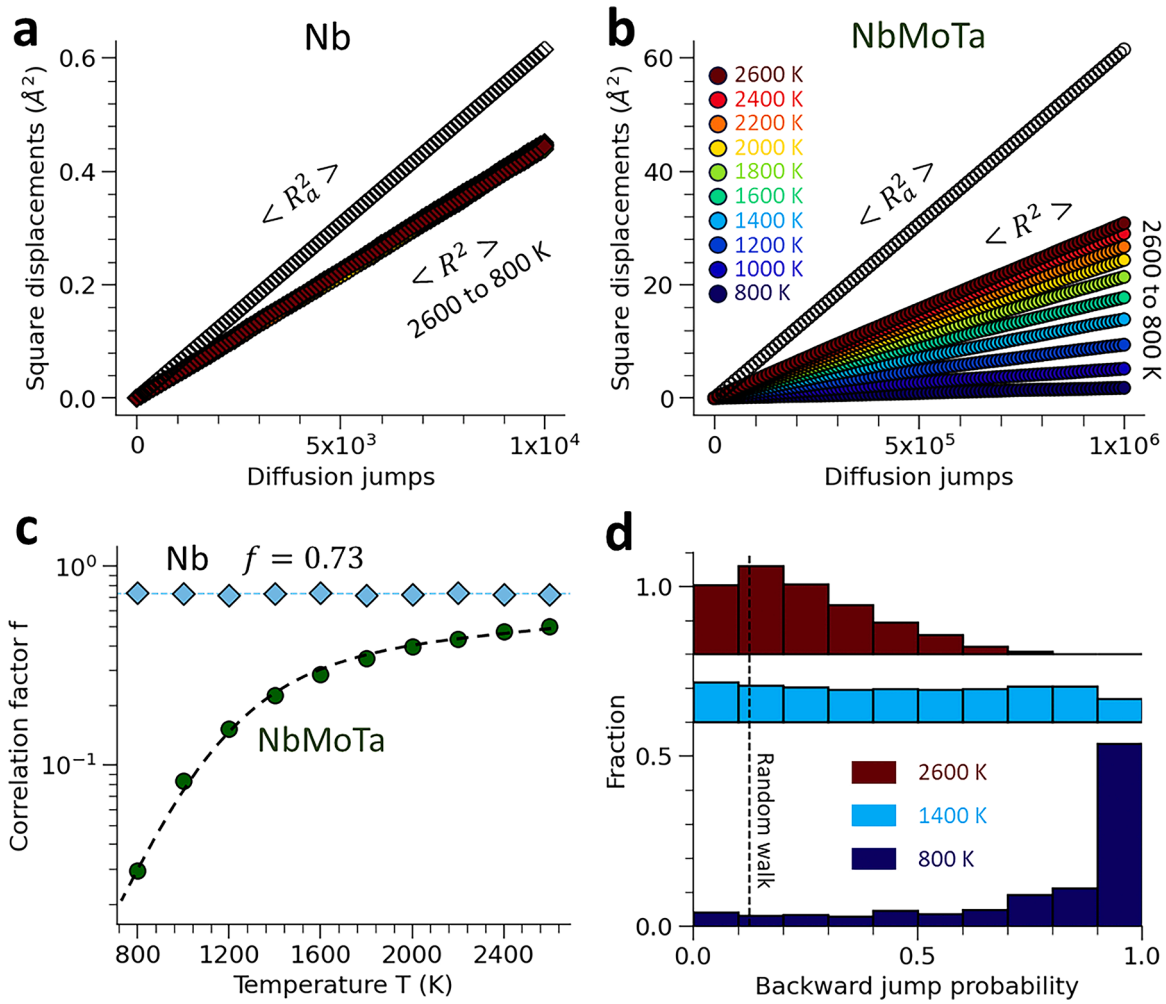

Fig. 5. Vacancy diffusion correlation factor in Nb and NbMoTa. (a-b) The curves of mean square displacement $\langle \boldsymbol{R}^2 \rangle$ and accumulative mean square displacement $\langle \boldsymbol{R}_a^2 \rangle$ as a function of vacancy jumps for temperatures from 2600 to 800 K. (c) Variation of correlation factors $f = \langle \boldsymbol{R}^2 \rangle / \langle \boldsymbol{R}_a^2 \rangle$ with temperature. (d) Fraction of backward jump probabilities for NbMoTa at 2600, 1400 and 800 K, indicating more frequent backward jumps at lower temperatures.

activation theory, $D(T) = D_0 exp(-\Delta G_m / k_B T)$. In this equation, ΔG_m, is the activation diffusion barrier (equal to the vacancy migration barrier ΔE_m for pure metals) and D_0 is the characteristic diffusivity, govern by material structure. In MPEAs, however, the vacancy migration barrier (ΔE_m) has a broad spectrum, rather than a constant value. The key question is how to extract the effective diffusion barrier ΔG_m from a spectrum. This barrier spectrum is an intrinsic material constant that is determined by alloy composition. As the diffusion correlation factor f in MPEAs varies with temperature, a revised diffusivity equation for MPEAs would take the form $D(T) = f(T) D_0 exp(-\Delta G_m / k_B T)$, with $D_0 = \lambda^2 Z \nu_0 / 6$. With the obtained temperature-dependent diffusion correlation factor $f(T)$, we can then compute ΔG_m if the diffusivity $D(T)$ is available. According to the Einstein-Smoluchowski equation [37,38], the diffusivity, which is a function of the mean square displacement $\langle \boldsymbol{R}^2 \rangle$ and time t, $D = \langle \boldsymbol{R}^2 \rangle / 6t$, can be computed from our neural network kinetic Monte Carlo simulations.

In Fig. 6a, we present the variation of mean square displacement $\langle \boldsymbol{R}^2 \rangle$ as a function of diffusion time at 2600, 1600, and 800 K for Nb, obtained from neural network kinetics simulations. While all simulations reach the same MSD of 0.5 $Å^2$, for pure Nb the required time at lower temperatures increases dramatically (exponentially). In the case of NbMoTa (Fig. 6b), the $\langle \boldsymbol{R}^2 \rangle$ gradually decreases at lower temperatures for the same number of one million jumps, which is also accompanied by an increase in diffusion time. Having obtained the diffusivity (Fig. 7a) and correlation factor (Fig. 5c), we derive the effective activation barrier for diffusion of the two materials at various temperatures, shown in Fig. 7b. In contrast to a constant ΔG_m around 1.05 eV for Nb, the diffusion activation barrier exhibits a clear temperature dependence for NbMoTa, decreasing from 1.65 eV at 2600 K to 1.46 eV at 800 K. This temperature dependence of effective diffusion barrier is intriguing, as it should be related to the vacancy migration barrier spectrum. For vacancy diffusion in pure metals, each jump direction will have the same migration barrier, leading to a constant activation diffusion barrier at the system level. In MPEAs, the distribution of vacancy migration barriers and system temperature influences the probability of diffusion pathway being picked. Fig. 7c presents the probability density distribution of the visited migration barriers at 800, 1400, and 2600 K. These diffusion-selected barriers show a temperature dependence and, with decreasing temperature, they shift to a smaller value (Fig. 7d). In Fig. 7e, we illustrate these visited barriers in terms of the portion in all available vacancy migration barriers (i.e., the full spectrum of barrier). It can be seen that, with decreasing temperature, these barriers decrease and concentrate in the left corner of the spectrum, indicating the lower barrier options are preferentially picked.

Unlike pure metals, the local chemical fluctuations in MPEAs result in a rugged diffusion energy landscape accompanied by a broad intrinsic migration barrier spectrum. As temperatures decrease, the vacancy jumps progressively select the low barriers, thereby reducing the effective activation barrier ΔG_m. This temperature dependence of ΔG_m and

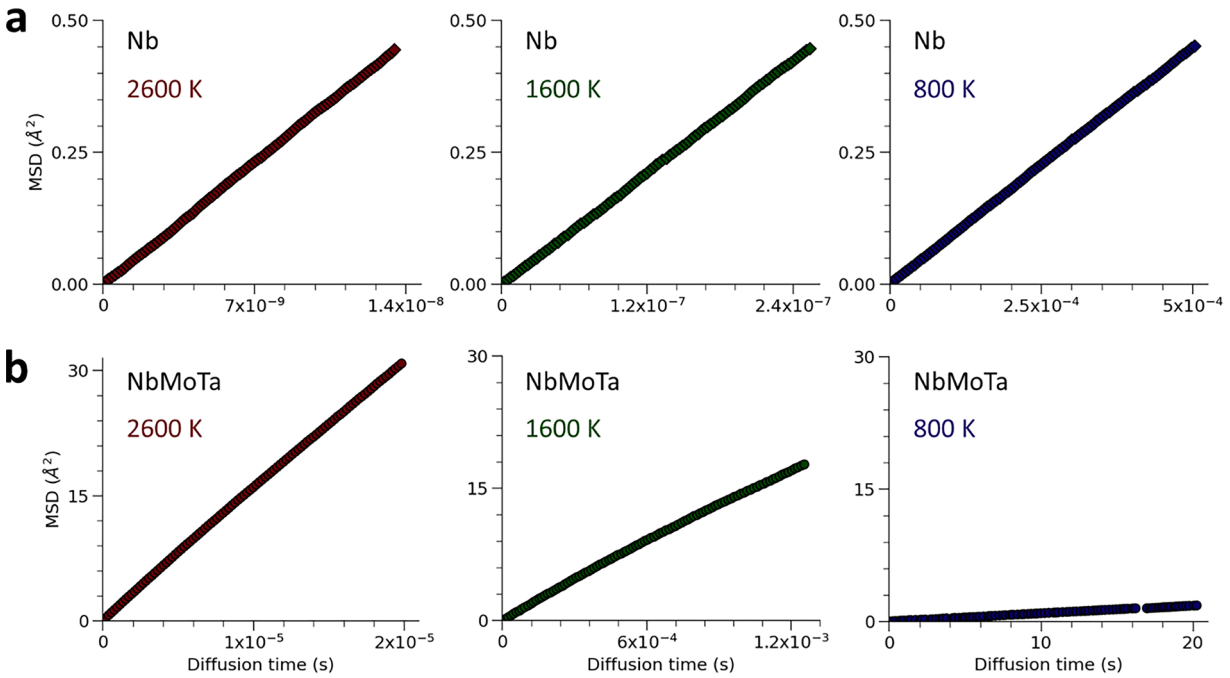

Fig. 6. The Mean Square Displacement (MSD) plotted as a function of time for three different temperatures: 2600, 1600, and 800 K. Figure (a) presents the data for pure Nb (niobium), while Figure (b) shows the same for the equiatomic MPEA NbMoTa.

the diffusion correlation factor f is considered the prominent characteristic of diffusion in MPEAs. This feature, which differentiates MPEAs from traditional metals such as pure metals and dilute alloys, should be responsible for abnormal diffusion behaviors when they occur.

5. The role of chemical complexity on diffusion barrier and diffusivity

Variations to overall alloy composition and local chemical ordering should influence the intrinsic vacancy migration barrier spectrum and hence diffusivity. To illustrate the effect of chemical composition on vacancy diffusion, we study and discuss three characteristic compositions: equimolar NbMoTa, non-equimolar $Nb_{10}Mo_{70}Ta_{20}$, and binary $Nb_{65}Mo_{35}$. Fig. 8a shows the corresponding vacancy diffusion barrier spectra, with indications of mean, $\overline{E}$, and standard deviation, σ. In these alloys, $Nb_{10}Mo_{70}Ta_{20}$ exhibits the highest $\overline{E}$ (1.92 eV) followed by NbMoTa (1.77 eV) and then $Nb_{65}Mo_{35}$ (1.63 eV). Concerning σ, $Nb_{65}Mo_{35}$ possesses the largest value (0.33 eV) followed by NbMoTa (0.26 eV) and $Nb_{10}Mo_{70}Ta_{20}$ (0.17 eV). Fig. 8b presents the diffusivity as a function of inverse temperature ($1/T$) for these alloys, indicating an increase in diffusion rate from $Nb_{10}Mo_{70}Ta_{20}$ to NbMoTa to $Nb_{65}Mo_{35}$. The influence of diffusion barrier spectrum on the diffusion correlation factor is presented in Fig. 8c for the three alloys. The $Nb_{65}Mo_{35}$ exhibits the smallest correlation factor (highest diffusion correlation), followed by NbMoTa and then $Nb_{10}Mo_{70}Ta_{20}$. This trend of f follows the barrier variance σ, implying that a larger σ (a rougher diffusion energy landscape) results in an enhancing diffusion correlation. Concerning the effective diffusion barrier ΔG_m, the $Nb_{10}Mo_{70}Ta_{20}$ is the highest and $Nb_{65}Mo_{35}$ is the lowest, indicating a positive relationship between mean vacancy barrier $\overline{E}$ and effective barrier ΔG_m.

Having demonstrated the composition-dependent diffusivity and its dependence on the diffusion barrier spectrum, we next perform extensive vacancy diffusion simulations for the entire ternary Nb-Mo-Ta space, aiming to understand the influence of chemical complexity. First, to illustrate the degree of chemical complexity, we adopt the conventional indicator of configurational entropy [18], which is defined as $S = -R\sum_{i=1}^{N} x_i \ln x_i$ where R is the gas constant and x_i is the concentration of element i. Fig. 9a illustrates a three-fold symmetric configurational entropy map, showing the highest chemical complexity being in the center (equimolar concentration). Fig. 9b shows the diffusivities (scaled by the diffusivity of pure Mo), obtained from one million diffusion jumps of neural network kinetics simulation at an intermediate temperature of 1600 K. Mo is chosen as the reference point due to its lowest vacancy diffusivity among the three pure elements. It is found that the composition with the lowest vacancy diffusivity is $Nb_5Mo_{65}Ta_{30}$, clearly deviating from the equimolar concentration. This suggests that the diffusivity is not simply determined by the configurational entropy, but its underlying diffusion barrier spectrum. When comparing the alloy diffusivity with pure Mo, as indicated by Fig. 9c, we can see that a large region of the composition space can have a higher diffusivity than Mo (red-colored region), indicating the sluggish diffusion is not generic since the alloys can have rapid diffusion than its constituent metals.

The inherent diffusion barrier spectrum, described by σ and $\overline{E}$ here, determines the two key parameters for diffusion, the diffusion correlation factor f and activation energy ΔG_m. A composition possessing a high $\overline{E}$ value leads to a high ΔG_m (low diffusivity). A large variance σ, suggesting a more rugged diffusion energy landscape, gives rise to a reduced f, or more correlated diffusion. Interestingly, diffusion correlation factor f can have a substantial influence on the diffusion rate. For example, the $Nb_5Mo_{65}Ta_{30}$ alloy displays a lower diffusion rate compared to the $Nb_{10}Mo_{70}Ta_{20}$ alloy. However, if the factor f is not considered, the diffusivity of $Nb_5Mo_{65}Ta_{30}$ would consistently, yet inaccurately, be perceived as higher.

6. Short- and long-range chemical order localizing vacancy diffusion

Originating from the attraction or repulsion among the constituent elements of MPEAs, vacancy diffusion leads to the emergence of chemical order in various length scales, such as long-range or short-range. The emergence of chemically ordered structures presumably impacts diffusion. To elucidate the influence of chemical order, we examine vacancy diffusion in two alloy systems: binary MoTa, which can exhibit long-range order (LRO), and the ternary NbMoTa carrying short-

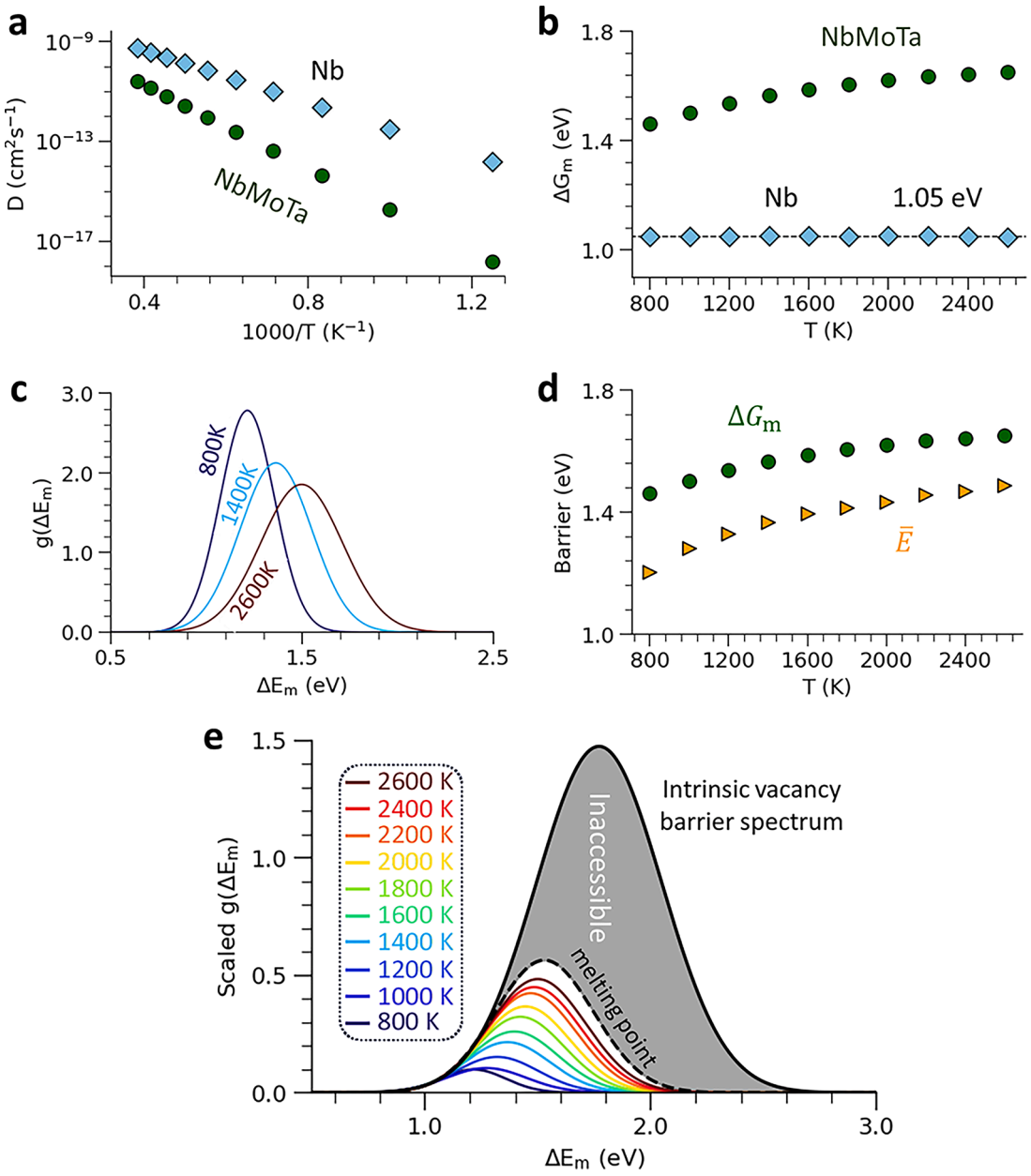

Fig. 7. The effective diffusion barrier in Nb and NbMoTa. (a) Vacancy diffusivity D as a function of $1000/T$ for Nb and NbMoTa. (b) The effective activation diffusion barrier ΔG_m for the two systems. (c) Probability density function of visited migration barriers $g(\Delta E_m)$ shifts negatively with decreasing temperature. (d) Temperature dependence of the mean visited barriers $\overline{E}$ and the effective diffusion barriers ΔG_m. (e) The portion of vacancy diffusion barrier spectrum visited at different temperatures. As temperature decreases, the accessible (visited) barriers drifts to the lower end of the intrinsic spectrum (black curve).

range order (SRO).

We have readied two states of MoTa, one being a random solid solution and the other showcasing a complete Mo-Ta B2 order, indicative of chemical LRO. Fig. 10a shows the diffusion trajectories in the random solution after 400 atomic jumps. As the temperature decreases from 3000 to 1000 K, the trajectories become increasingly shortened. This is also evidenced by the mean squared displacement, $\langle \boldsymbol{R}^2 \rangle$. Intriguingly, the diffusion trajectories in the B2 ordered alloy become even more localized, accompanied by decreases in $\langle \boldsymbol{R}^2 \rangle$ (Fig. 10b). Notably, the $\langle \boldsymbol{R}^2 \rangle$ and diffusion trajectory in the ordered system at 1000 K are nearly zero after 400 jumps, indicating the vacancy is completely trapped in a local region. In Fig. 11a, we compare the temperature-dependent diffusivity for the two systems, demonstrating the effect of chemical LRO on lowering diffusion rate. This reduction becomes increasingly pronounced with decreasing temperature, which should own to change in the correlation factor and effective activation barrier. Fig. 11b depicts the correlation factors for both the random and long-range B2-ordered systems, with the value decreasing by four orders of magnitude in the B2-ordered system compared to a decrease by two orders in the random alloy. Fig. 11c presents the variation of effective diffusion barrier with temperature. The decrease in the diffusion barrier with temperature in the ordered system results from the disruption of the B2 order due to vacancy diffusion.

After introducing chemical SRO into the NbMoTa alloy through neural network kinetics simulation, we further study its effect on vacancy diffusion. Fig. 12a-b present the diffusion behaviors for the random and short-range ordered systems after 400 jumps. In contrast to MoTa, the effect of chemical short-range order on diffusion is less significant, though still observable. As shown in Fig. 13a, the diffusivity of SRO exhibits lower values, especially at lower temperatures (note that

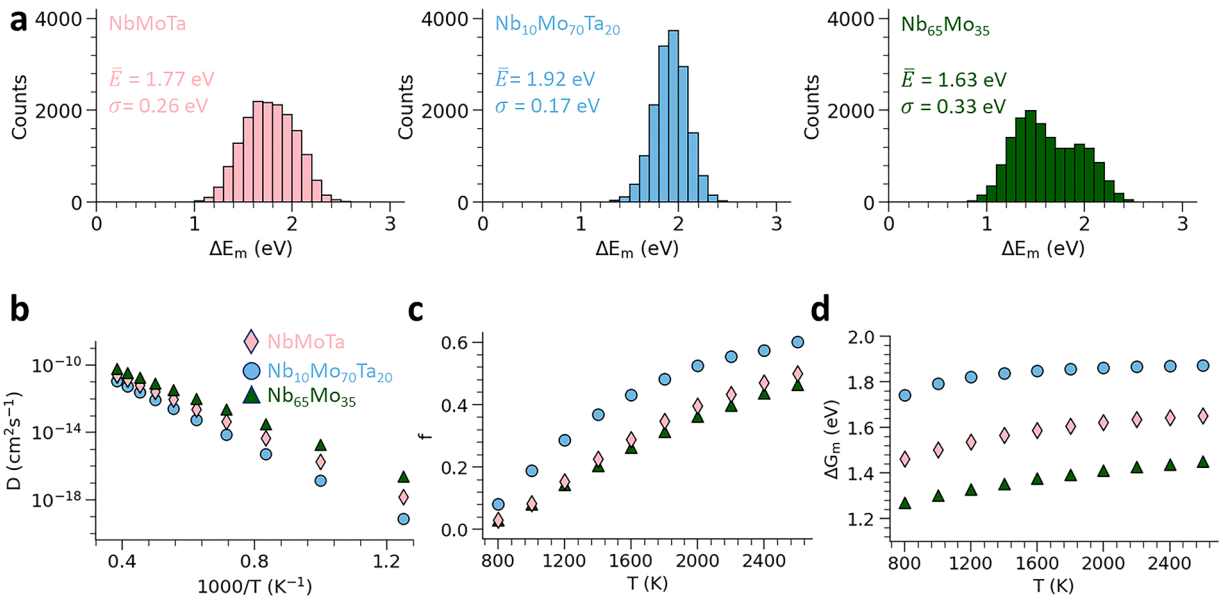

Fig. 8. Migration barrier spectrums and vacancy diffusion behaviors in three representative alloys. (a) Migration barrier spectrums in equimolar NbMoTa, $Nb_{10}Mo_{70}Ta_{20}$, and $Nb_{65}Mo_{35}$ alloys. $\bar{E}$ and σ indicate mean and standard deviation, respectively. (b-d) Diffusivity D, diffusion correlation factor f, and effective diffusion barrier ΔG_m in three alloys at different temperatures.

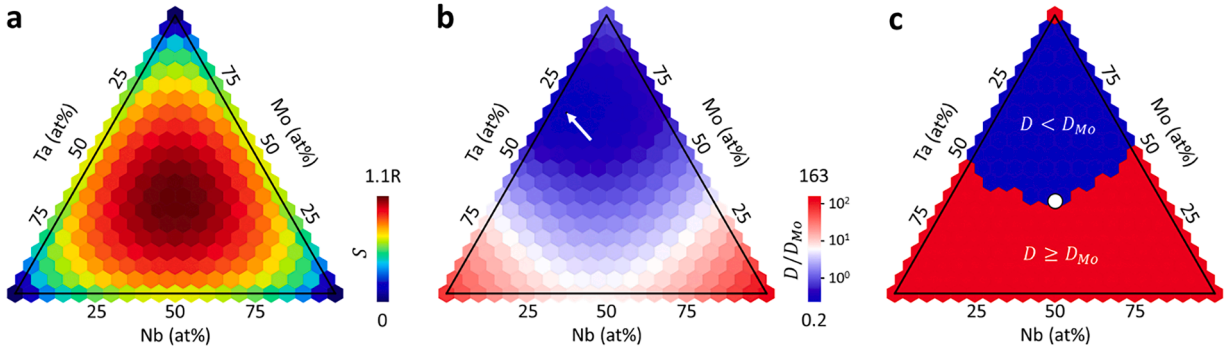

Fig. 9. Vacancy diffusivity across the entire ternary space of NbMoTa alloys. (a) presents the configurational entropy, highlighting that the region of equimolar concentration located at the center. (b) shows the computed diffusivity D, revealing the lowest diffusivity at 1600 K occurs for $Nb_5Mo_{65}Ta_{30}$ (marked by the arrow). (c) depicts the composition region possessing higher (red color) and lower (blue colors) diffusivity than that of Mo. The equimolar NbMoTa, marked by a white dot, displays a lower diffusivity than its constituent element, Mo.

the diffusivity is plotted using a logarithmic scale). This SRO-lowered diffusivity originates from the enhanced diffusion correlation (Fig. 13b) and increased diffusion barrier (Fig. 13c). Through a comparative analysis of MoTa and NbMoTa, we infer that chemical ordering diminishes diffusion. The degree of this reduction is dependent on both the extent and range (long or short) of the chemical order.

7. Discussion and conclusions

Vacancy diffusion, which governs many kinetic processes, such as precipitation [39], segregation [40], and radiation defect annihilation [41], is particularly complex in MPEAs. This complexity, originating from local chemical fluctuations, give rise to a salient feature related to vacancy diffusion barrier—a spectral distribution [7–9]. This diffusion barrier spectrum is an inherent material constant akin to modulus, which is determined by the composition of crystalline alloy. The presence of a broad spectrum of diffusion barriers influences the probability of vacancy jumps along each pathway, leading to non-random vacancy diffusion. Unlike pure metals and dilute alloys, the diffusion activation (effective) barrier ΔG_m and correlation factor f in multicomponent alloys are not constant, instead, they can substantially decrease with lowering the system temperature. The decrease in the ΔG_m can be understood from the increased propensity towards pathways with lower barriers. As the temperature drops, vacancies favor pathways with lower barriers, which skews the visited barriers towards the lower end of the spectrum, leading to a reduced effective barrier ΔG_m. This preferentially pathway selection inevitably affects the randomness of vacancy diffusion and the correlation factor f. As the number of activated pathways diminishes with decreasing temperature, vacancy jumps become more concentrated along lower energy pathways, resulting in more coordinated jumps (a lower value of f). From a theoretical perspective, the correlation factor is estimated as $f = 1 - 2/Z$, where Z denotes the coordination number, equivalent to the number of jump pathways for vacancy [4]. For a pure bcc metal, all pathways have the same jump

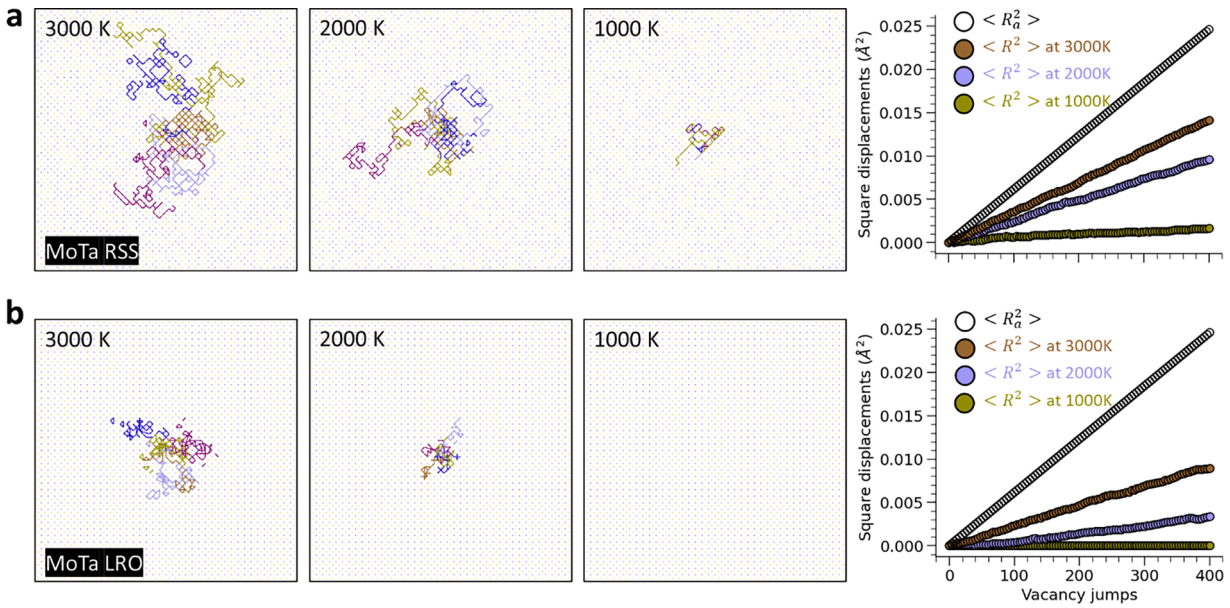

Fig. 10. Vacancy diffusion trajectories over 400 atom jumps and the corresponding square displacement relationship at temperatures of 3000, 2000 and 1000 K. (a) presents data for MoTa with random solid solution, and (b) is for MoTa with long-range B2 order.

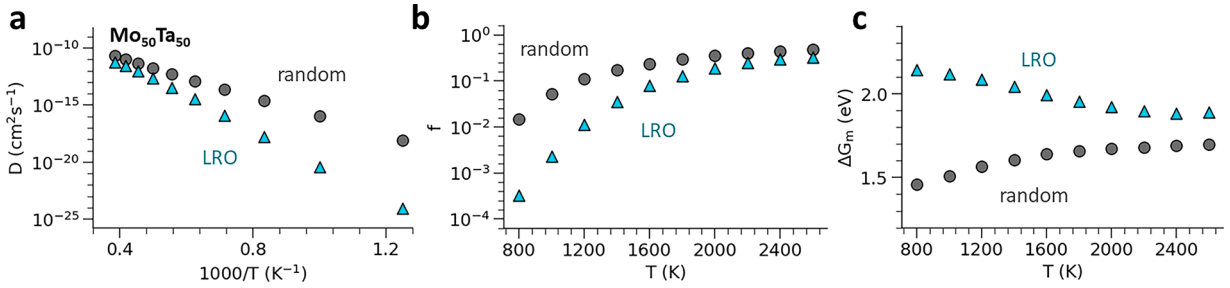

Fig. 11. (a) Comparison of vacancy diffusivity for random and long-range ordered (LRO) MoTa. (b-c) shows the reduced diffusion correlation factor f and enhanced effective activation diffusion barrier ΔG_m in the LRO alloy, accounting for the reduced diffusivity.

probability and $Z = 8$. Within multicomponent alloys, the number of available pathways decreases as temperature decreases, effectively reducing Z at lower temperatures, thereby accounting for the decreased correlation factor. In the extreme scenario of one-dimensional diffusion, where Z equals 2, the value of f reduces to zero.

The MPEAs containing a larger number of equimolar elements (higher configuration entropy) are typically thought to exhibit slow diffusion rates. The "sluggish diffusion" considered to be characteristic of MPEAs has sparked an interesting debate for a decade. Particularly in face-centered cubic alloys, various theories and models, such as percolation theory, were developed to explain sluggish diffusion in concentrated binary alloys [42,43]. By sampling the diffusion rate throughout the entire compositional range of NbMoTa alloys, we found, intriguingly, that the alloy with the slowest diffusion situates in the non-equimolar region. Different from the configurational entropy aspect, we propose that the rate of diffusion is governed by the inherent vacancy migration barrier spectrum. In multicomponent alloys, the composition with a higher mean barrier introduces a larger effective diffusion barrier, leading to a reduction in the rate of vacancy jumps. A greater variance in the barrier spectrum, indicating a more rugged diffusion energy landscape, makes a more correlated vacancy jumps, hence a lowered diffusivity.

As an emerging class of material systems, refractory MPEAs have attracted growing attention from the community due to their intriguing properties such as high-temperature strength [18,10] and high radiation resistance [44]. The evolution of these alloys opens up exciting opportunities for understanding and utilizing the vast design space along the composition dimension. Harnessing such space is of utmost significance as the alloys with non-equimolar concentrations typically can exhibit superior mechanical performance compared to their equimolar counterparts [10,45]. Here, we demonstrate an application of neural network framework that couples with machine learning and atomics simulations to efficiently predict vacancy diffusivity in the complete space of a ternary alloy. It is worth noting that different encoding methods, including coordinate system transformation [46,47] and local atomic configuration [48], have been proposed to predict vacancy diffusion in concentrated alloys. The neuron map (on-lattice) representation of atomic structure and chemistry [31] has dimensionality $O(N)$, which scales linearly with the number of atoms N, and has the lowest dimensionality possible as a crystal descriptor. The model exhibits high accuracy in barrier prediction. For instance, the mean absolute errors (MAE) for dilute solution $Nb_{10}Mo_{10}Ta_{80}$ and concentrated solution $Nb_{20}Mo_{60}Ta_{20}$ are 0.019 and 0.024 eV, respectively. The error is smaller than 1.4 % of the true diffusion barrier [31]. With the rapid advancements of machine learning techniques for complex systems, such as autoencoder [49], generative model [50], and transformer [51], learning and predicting defects and their controlling properties in the entire refractory groups may soon become a plausible reality.

In summary, we examine vacancy diffusion in multicomponent Nb-Mo-Ta alloys using network-based kinetic Monte Carlo simulations. It is found the diffusion correlation factor f and activation energy ΔG_m are not constants in these alloys; rather, they exhibit a significant decrease

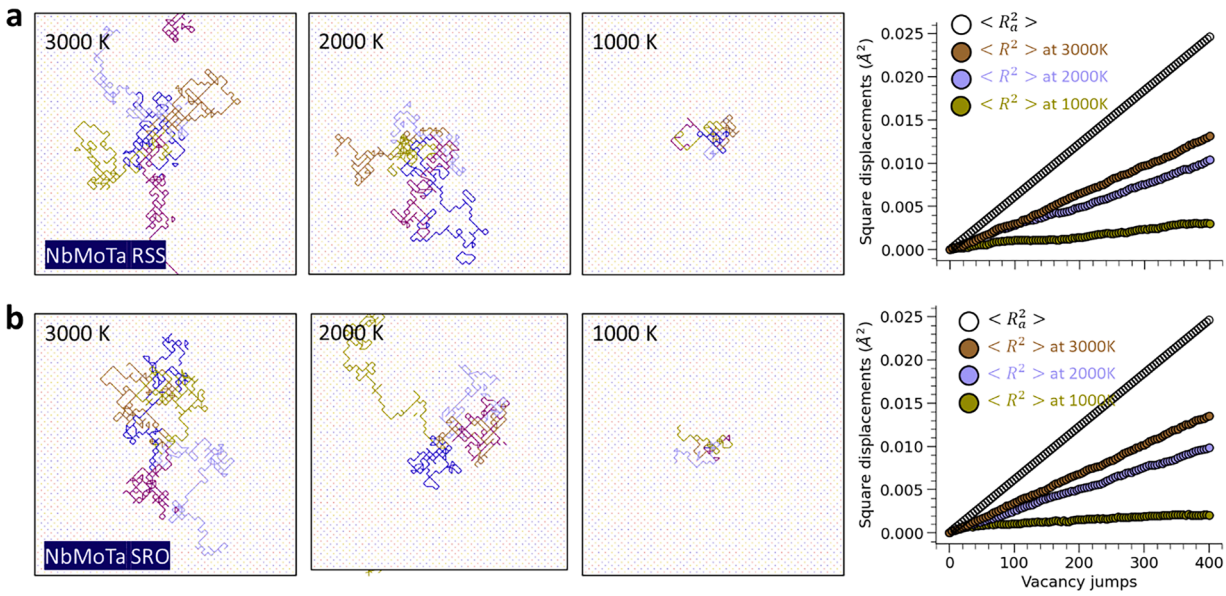

Fig. 12. Vacancy diffusion trajectories with 400 atom jumps and the corresponding square displacement relationship at temperatures of 3000, 2000, and 1000 K. (a) presents data for ternary NbMoTa with random solid solution, and (b) is for NbMoTa with short-range order (SRO).

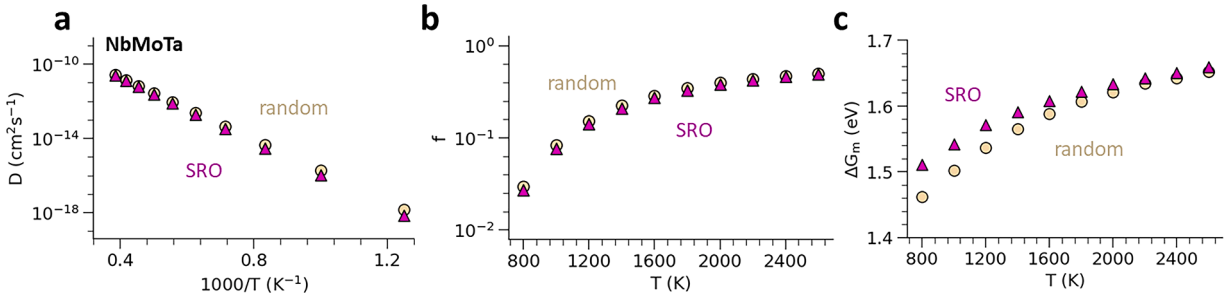

Fig. 13. (a) Comparison of vacancy diffusivity for random and SRO NbMoTa. (b-c) illustrates the reduced diffusion correlation factor and enhanced effective activation diffusion barrier in the SRO system.

with decreasing temperatures. By efficiently sampling vacancy diffusivity in the entire compositional space, we discover the slowest vacancy diffusion surprisingly occurs in the non-equimolar region, rather than the equimolar concentration. These interesting observations arise from the vacancy barrier spectrum that multicomponent alloys inherently hold. In the presence of chemical short-range order in NbMoTa alloy, vacancy diffusion exhibits a considerable decrease. This reduction in diffusion becomes particularly pronounced in MoTa alloys possessing long-range B2 order.

Code availability

The source code of NNK to perform the kinetics simulations is available at https://github.com/UCICaoLab/NKK.

Declaration of competing interest

The authors declare that they have no known competing financial interests or personal relationships that could have appeared to influence the work reported in this paper.

Acknowledgments

This research was supported by the U.S. Department of Energy, Office of Science, Basic Energy Sciences, under Award No. DE-SC0022295. T.J.R was supported by the U.S. Department of Energy, Basic Energy Sciences, under Award No. DE-SC0021224.

References

[1] W. Sun, Y. Zhu, R. Marceau, L. Wang, Q. Zhang, X. Gao, C. Hutchinson, Precipitation strengthening of aluminum alloys by room-temperature cyclic plasticity, 2019. https://www.science.org.
[2] S.H. Kim, H. Kim, N.J. Kim, Brittle intermetallic compound makes ultrastrong low-density steel with large ductility, Nature 518 (2015) 77–79, https://doi.org/10.1038/nature14144.
[3] C. Lu, L. Niu, N. Chen, K. Jin, T. Yang, P. Xiu, Y. Zhang, F. Gao, H. Bei, S. Shi, M. R. He, I.M. Robertson, W.J. Weber, L. Wang, Enhancing radiation tolerance by controlling defect mobility and migration pathways in multicomponent single-phase alloys, Nat. Commun. 7 (2016) 13564, https://doi.org/10.1038/ncomms13564.
[4] H. Mehrer, Diffusion in solids: fundamentals, methods, materials, diffusion-controlled processes. Springer Series in Solid-State Sciences 155, 2007. ISSN: 9783540714866.
[5] M. Jin, P. Cao, M.P. Short, Thermodynamic mixing energy and heterogeneous diffusion uncover the mechanisms of radiation damage reduction in single-phase Ni-Fe alloys, Acta Mater. 147 (2018) 16–23, https://doi.org/10.1016/j.actamat.2017.12.064.

[6] P. Cao, How does short-range order impact defect kinetics in irradiated multiprincipal element alloys? Acc. Mater. Res. 2 (2021) 71–74, https://doi.org/10.1021/accountsmr.0c00102.

[7] B. Xing, X. Wang, W.J. Bowman, P. Cao, Short-range order localizing diffusion in multi-principal element alloys, Scr. Mater. 210 (2022), https://doi.org/10.1016/j.scriptamat.2021.114450.

[8] Z. Fan, B. Xing, P. Cao, Predicting path-dependent diffusion barrier spectra in vast compositional space of multi-principal element alloys via convolutional neural networks, Acta Mater. 237 (2022), https://doi.org/10.1016/j.actamat.2022.118159.

[9] X. Wang, F. Maresca, P. Cao, The hierarchical energy landscape of screw dislocation motion in refractory high-entropy alloys, Acta Mater. 234 (2022) 118022, https://doi.org/10.1016/j.actamat.2022.118022.

[10] E.P. George, D. Raabe, R.O. Ritchie, High-entropy alloys, Nat. Rev. Mater. 4 (2019) 515–534, https://doi.org/10.1038/s41578-019-0121-4.

[11] D.B. Miracle, High entropy alloys as a bold step forward in alloy development, Nat. Commun. 10 (2019) 1805, https://doi.org/10.1038/s41467-019-09700-1.

[12] B. Cantor, I.T.H. Chang, P. Knight, A.J.B. Vincent, Microstructural development in equiatomic multicomponent alloys, Mater. Sci. Eng. A 375-377 (2004) 213–218, https://doi.org/10.1016/j.msea.2003.10.257.

[13] J.W. Yeh, S.K. Chen, S.J. Lin, J.Y. Gan, T.S. Chin, T.T. Shun, C.H. Tsau, S.Y. Chang, Nanostructured high-entropy alloys with multiple principal elements: novel alloy design concepts and outcomes, Adv. Eng. Mater. 6 (2004) 299–303, https://doi.org/10.1002/adem.200300567.

[14] O.N. Senkov, G.B. Wilks, J.M. Scott, D.B. Miracle, Mechanical properties of Nb25Mo25Ta25W25 and V20Nb20Mo20Ta20W20 refractory high entropy alloys, Intermetallics (Barking) 19 (2011) 698–706, https://doi.org/10.1016/j.intermet.2011.01.004.

[15] F. Wang, G.H. Balbus, S. Xu, Y. Su, J. Shin, P.F. Rottmann, K.E. Knipling, J. C. Stinville, L.H. Mills, O.N. Senkov, I.J. Beyerlein, T.M. Pollock, D.S. Gianola, Multiplicity of dislocation pathways in a refractory multiprincipal element alloy, Science (1979) 370 (2020) 95–101, https://doi.org/10.1126/science.aba3722.

[16] H. Luo, Z. Li, A.M. Mingers, D. Raabe, Corrosion behavior of an equiatomic CoCrFeMnNi high-entropy alloy compared with 304 stainless steel in sulfuric acid solution, Corros. Sci. 134 (2018) 131–139, https://doi.org/10.1016/j.corsci.2018.02.031.

[17] N.A.P.K. Kumar, C. Li, K.J. Leonard, H. Bei, S.J. Zinkle, Microstructural stability and mechanical behavior of FeNiMnCr high entropy alloy under ion irradiation, Acta Mater. 113 (2016) 230–244, https://doi.org/10.1016/j.actamat.2016.05.007.

[18] D.B. Miracle, O.N. Senkov, A critical review of high entropy alloys and related concepts, Acta Mater. 122 (2017) 448–511, https://doi.org/10.1016/j.actamat.2016.08.081.

[19] K.Y. Tsai, M.H. Tsai, J.W. Yeh, Sluggish diffusion in Co–Cr–Fe–Mn–Ni high-entropy alloys, Acta Mater. 61 (2013) 4887–4897, https://doi.org/10.1016/j.actamat.2013.04.058.

[20] A. Paul, Comments on “Sluggish diffusion in Co–Cr–Fe–Mn–Ni high-entropy alloys” by K.Y. Tsai, M.H. Tsai and J.W. Yeh, Acta Materialia 61 (2013) 4887-4897, Scr. Mater. 135 (2017) 153–157, https://doi.org/10.1016/j.scriptamat.2017.03.026.

[21] K.Y. Tsai, M.H. Tsai, J.W. Yeh, Reply to comments on “Sluggish diffusion in Co-Cr-Fe-Mn-Ni high-entropy alloys” by K.Y. Tsai, M.H. Tsai and J.W. Yeh, Acta Materialia 61 (2013) 4887-4897, Scr. Mater. 135 (2017) 158–159, https://doi.org/10.1016/j.scriptamat.2017.03.028.

[22] J. Dąbrowa, M. Zajusz, W. Kucza, G. Cieślak, K. Berent, T. Czeppe, T. Kulik, M. Danielewski, Demystifying the sluggish diffusion effect in high entropy alloys, J. Alloys Compd. 783 (2019) 193–207, https://doi.org/10.1016/j.jallcom.2018.12.300.

[23] W. Kucza, J. Dąbrowa, G. Cieślak, K. Berent, T. Kulik, M. Danielewski, Studies of “sluggish diffusion” effect in Co-Cr-Fe-Mn-Ni, Co-Cr-Fe-Ni and Co-Fe-Mn-Ni high entropy alloys; determination of tracer diffusivities by combinatorial approach, J. Alloys Compd. 731 (2018) 920–928, https://doi.org/10.1016/j.jallcom.2017.10.108.

[24] A. Seoane, D. Farkas, X.M. Bai, Influence of compositional complexity on species diffusion behavior in high-entropy solid-solution alloys, J. Mater. Res. 37 (2022) 1403–1415, https://doi.org/10.1557/s43578-022-00545-x.

[25] D.L. Beke, G. Erdélyi, On the diffusion in high-entropy alloys, Mater. Lett. 164 (2016) 111–113, https://doi.org/10.1016/j.matlet.2015.09.028.

[26] Y.Z. Wang, Y.J. Wang, Disentangling diffusion heterogeneity in high-entropy alloys, Acta Mater. 224 (2022) 117527, https://doi.org/10.1016/J.ACTAMAT.2021.117527.

[27] Y.N. Osetsky, L.K. Béland, A.V. Barashev, Y. Zhang, On the existence and origin of sluggish diffusion in chemically disordered concentrated alloys, Curr. Opin. Solid State Mater. Sci. 22 (2018) 65–74, https://doi.org/10.1016/j.cossms.2018.05.003.

[28] Y. Osetsky, A.V. Barashev, L.K. Béland, Z. Yao, K. Ferasat, Y. Zhang, Tunable chemical complexity to control atomic diffusion in alloys, npj Comput. Mater. 6 (2020) 38, https://doi.org/10.1038/s41524-020-0306-9.

[29] S.L. Thomas, S. Patala, Vacancy diffusion in multi-principal element alloys: the role of chemical disorder in the ordered lattice, Acta Mater. 196 (2020) 144–153, https://doi.org/10.1016/j.actamat.2020.06.022.

[30] J.P. Du, P. Yu, S. Shinzato, F. Meng, Y. Sato, Y. Li, Y. Fan, O. Shigenobu, Chemical domain structure and its formation kinetics in CrCoNi medium-entropy alloy, Acta Mater/ 240 (2022) 118314.

[31] B. Xing, T.J. Rupert, X. Pan, P. Cao, Neural network kinetics: diffusion multiplicity and b2 ordering in compositionally complex alloys, Preprint, ArXiv.2304.02957. (2023). 10.48550/arXiv.2304.02957.

[32] G. Henkelman, B.P. Uberuaga, H. Jónsson, Climbing image nudged elastic band method for finding saddle points and minimum energy paths, J. Chem. Phys. 113 (2000) 9901–9904, https://doi.org/10.1063/1.1329672.

[33] S. Yin, Y. Zuo, A. Abu-Odeh, H. Zheng, X.G. Li, J. Ding, S.P. Ong, M. Asta, R. O. Ritchie, Atomistic simulations of dislocation mobility in refractory high-entropy alloys and the effect of chemical short-range order, Nat. Commun. 12 (2021), https://doi.org/10.1038/s41467-021-25134-0.

[34] D.T. Gillespie, A general method for numerically simulating the stochastic time evolution of coupled chemical reactions, 1976.

[35] R.R. Rao, C.S. Menon, E.S. Fisher, C.J. Henken, M.H. Manghnani, J. Phys Chem, B. Srinivasan, R. Ramji Rao, R. Bamji Rao, H.F. Bezdek, R.E. Schmunk, L. Finegold, P. Status Solidi, B. Bamji Bao, R. Srinivasan, Integral methods in the calculation of correlation factors in diffusion, 1971, J. Appl. Phys. 33 (1972) 491. B. Bamji Rao, G.L. Montet, Solids.

[36] G.S. Was, Radiation Materials Science, Springer, 2007.

[37] A. Einstein, Über die von der molekularkinetischen Theorie der Wärme geforderte Bewegung von in ruhenden Flüssigkeiten suspendierten Teilchen, Ann. Phys. 322 (1905) 549–560, https://doi.org/10.1002/andp.19053220806.

[38] M. von Smoluchowski, Zur kinetischen theorie der brownschen molekularbewegung und der suspensionen, Ann. Phys. 326 (1906) 756–780, https://doi.org/10.1002/andp.19063261405.

[39] Y. Yang, T. Chen, L. Tan, J.D. Poplawsky, K. An, Y. Wang, G.D. Samolyuk, K. Littrell, A.R. Lupini, A. Borisevich, E.P. George, Bifunctional nanoprecipitates strengthen and ductilize a medium-entropy alloy, Nature 595 (2021) 245–249, https://doi.org/10.1038/s41586-021-03607-y.

[40] L. Li, Z. Li, A. Kwiatkowski da Silva, Z. Peng, H. Zhao, B. Gault, D. Raabe, Segregation-driven grain boundary spinodal decomposition as a pathway for phase nucleation in a high-entropy alloy, Acta Mater. 178 (2019) 1–9, https://doi.org/10.1016/j.actamat.2019.07.052.

[41] J. Du, S. Jiang, P. Cao, C. Xu, Y. Wu, H. Chen, E. Fu, Z. Lu, Superior radiation tolerance via reversible disordering–ordering transition of coherent superlattices, Nat. Mater. (2022), https://doi.org/10.1038/s41563-022-01260-y.

[42] Y.N. Osetsky, L.K. Béland, R.E. Stoller, Specific features of defect and mass transport in concentrated fcc alloys, Acta Mater. 115 (2016) 364–371, https://doi.org/10.1016/j.actamat.2016.06.018.

[43] S. Zhao, Y. Osetsky, Y. Zhang, Diffusion of point defects in ordered and disordered Ni–Fe alloys, J. Alloys Compd. 805 (2019) 1175–1183, https://doi.org/10.1016/j.jallcom.2019.07.142.

[44] O. El-Atwani, N. Li, M. Li, A. Devaraj, J.K.S. Baldwin, M.M. Schneider, D. Sobieraj, J.S. Wróbel, D. Nguyen-Manh, S.A. Maloy, E. Martinez, Outstanding radiation resistance of tungsten-based high-entropy alloys, Sci. Adv. 5 (2019) eaav2002, https://doi.org/10.1126/sciadv.aav2002.

[45] Z. Li, K.G. Pradeep, Y. Deng, D. Raabe, C.C. Tasan, Metastable high-entropy dual-phase alloys overcome the strength-ductility trade-off, Nature 534 (2016) 227–230, https://doi.org/10.1038/nature17981.

[46] B. Xu, J. Zhang, S. Ma, Y. Xiong, S. Huang, J.J. Kai, S. Zhao, Revealing the crucial role of rough energy landscape on self-diffusion in high-entropy alloys based on machine learning and kinetic Monte Carlo, Acta Mater. 234 (2022), https://doi.org/10.1016/j.actamat.2022.118051.

[47] B. Xu, J. Zhang, Y. Xiong, S. Ma, Y. Osetsky, S. Zhao, Mechanism of sluggish diffusion under rough energy landscape, Cell Rep. Phys. Sci. 4 (2023), https://doi.org/10.1016/j.xcrp.2023.101337.

[48] W. Huang, X.M. Bai, Machine learning based on-the-fly kinetic Monte Carlo simulations of sluggish diffusion in Ni-Fe concentrated alloys, J. Alloys Compd. 937 (2023) 168457, https://doi.org/10.1016/j.jallcom.2022.168457.

[49] I. Tolstikhin, O. Bousquet, S. Gelly, B. Schölkopf, Wasserstein Auto-Encoders, (n. d.).

[50] B. Sanchez-Lengeling, A. Aspuru-Guzik, Inverse molecular design using machine learning: generative models for matter engineering, Science (1979) 361 (2018) 360–365, https://doi.org/10.1126/science.aat2663.

[51] A. Vaswani, N. Shazeer, N. Parmar, J. Uszkoreit, L. Jones, A.N. Gomez, Ł. Kaiser, I. Polosukhin, Attention is all you need, Adv. Neural. Inf. Process. Syst. (2017).